*S Samuel*
*Ocid Mursid*
*Serliana Yulianti*
*Kiryanto*
*Muhammad Iqbal*

http://dx.doi.org/10.21278/brod73306

ISSN 0007-215X
eISSN 1845-5859

# EVALUATION OF INTERCEPTOR DESIGN TO REDUCE DRAG ON PLANING HULL

UDC 629.5.015.2:629.5.022.1
Original scientific paper

**Summary**

A planing hull is a high-speed craft with relatively complex hydrodynamic characteristics. An increase in speed can induce a significant change in trim angle with an increment in ship drag. One solution to reduce ship resistance is to use an interceptor. This research aimed to analyze the hydrodynamics of a planing hull vessel by applying an interceptor. The fundamental aspects reviewed included the analysis of drag, trim, heave, and lift force. The interceptor would be investigated on the basis of its integrated position at its height. This research also used the computational fluid dynamic (CFD) method in calm water conditions. All simulations were conducted with the same mesh structure, which allowed the performance evaluation of the interceptor in calculating turbulent air–water flow around the ship. Numerical calculations used the Reynolds-averaged Navier–Stokes (RANS) equation with the k–ε turbulence model to predict the turbulent flow. The vertical motion of the ship was modeled using dynamic fluid–body interaction (DFBI) in the fluid domain through an overset mesh technique. The numerical approach was compared with the experimental test results of Park et al. to ensure the accuracy of the test results. The interceptor was designed at the transition phase, which showed the highest trim angle followed by high drag. The interceptor would experience negative trim at high speeds; thus, it was not recommended. The research results indicated that the most effective use of the interceptor was at Froude number 0.87 close to the chine position with a height of 100%. This interceptor could reduce a maximum of 57% drag, 17% heave, 8.48% trim, and 0.12% lift force. The interceptor could increase excessive drag and trim at Froude numbers over 1.16. The interceptor proved to be remarkably useful in trim control and ship drag reduction, but selecting the wrong dimensions and positions of the interceptor could endanger the ship. This simulation was performed on Aragon-2; thus, the interceptor performance may possibly change if a different hull geometry is used.

*Key words:* *planing hull; drag; heave; lift force; trim*

## 1. Introduction

Changes in trim angles and increased drag have crucial impacts on the performance of the planing hull. Some devices used to improve ship performance include hull vane, stern flap,

stern wedge, and others. According to Uithof [1], hull vanes can reduce the effects of waves and ship drag. Hongbo Hou et al. [2] reported that the lift created by the hull vane could reduce 3.7% of total drag and 26% of trim. The complexity of the hydrodynamic forces experienced by fast ships was closely related to changes in ship speed. However, the hull vane had limitations; that is, it could not synchronize its position to respond to changes in ship speed. Thus, the angle and position of the hull vane could not be modified. The effectiveness of the interceptors as trim controllers is not only confirmed, but is also quite significant when compared to bare hull performances at the best center of gravity position [3]. Other studies identify interceptors by comparing numerical simulation methods and experimental data. The results of the analysis show that the depth of the interceptor should be determined by the shape of the hull to achieve effective ship performance to reduce ship resistance [4].

The unique feature of the interceptor lies in its control system, which can change its position vertically. Several types of research have demonstrated the effectiveness of the interceptor in improving the hydrodynamic performance of high-speed planing craft. The interceptor was also used as a motion control to improve the motion response of the ship [5]. Another research compared the use of trim tabs and interceptors of the same size. The research was analyzed using CFD and showed that the pressure created by the interceptor was better than that of the trim tab [6]. Investigation of interceptors on high-speed craft showed that interceptors could increase the pressure and lift force followed by a reduction in trim angle [7]. Research on interceptors under regular head waves revealed that interceptors could reduce heave motion by 16% to 18% at Froude number 1.78 [8]. The effect of the interceptor is highly dependent on the geometry of the ship; thus, the analysis of the planing hull integrated with the interceptor depends on ship geometries. Considering the effect of the small dimensions, the interceptor can potentially be placed not only at the stern of the ship but also in the middle of the hull. The interceptor is also applied in the chine or keel area of the ship or between it. However, for practical and applicable use, this study examines the position of the interceptor in the stern area to avoid changes in hull construction. Considering the experimental study of the design of the interceptor dimensions, the interceptor can be applied close to chine, close to keel, and at mid-position areas.

Highlighting previous research, the interceptor showed different performances when used at various altitudes [9]. This research aimed to analyze the altitude and position of the interceptor against ship resistance. Furthermore, different speeds affected the hydrodynamic performance of the ship integrated with the interceptor. The interceptor created a balancing moment and changed the pressure distribution in the ship's stern. Therefore, changing the altitude and position of the interceptor impacted the drag, heave, trim, and lift force of the ship.

Yousefi et al. [10] reported three CFD methods related to ship planing hull, namely finite volume method (FVM), finite element method (FEM), and boundary element method (BEM). FVM was the most dominant method used to predict the characteristics of the planing hull ship because of its better accuracy compared with other methods. Research on FEM was successfully conducted in 2015 to predict catamaran drag by ignoring the motion of the ship [11]. The research was continued by modifying the addition of the center bulb to reduce the total resistance [12]. Another study stated similar results between CFD and experiments by reviewing the wave contour, pressure distribution, and resistance coefficient of the vessel [13]. Sukas et al. [14] conducted research using empirical, experimental, and CFD methods. They found that the CFD method with an overset grid could solve flow problems around the hull type planing at high speed. Numerical simulation research improved accuracy in resolving the flow around the hull. In addition, advances in computer technology could model and analyze complex hydrodynamic forces. Research with numerical methods facilitated economic research costs and took a relatively short time with practicality and efficiency. The current research used an interceptor analysis approach using a numerical simulation method based on FVM. The

FVM method used the RANS principle to describe turbulent flow through the water and air phases. Furthermore, this research verified the results of the CFD simulation using the findings of Park et al.'s [16] experiment in calm water conditions. The research results were expected to help ship designers to improve fuel efficiency.

## 2. Method

### 2.1 Research object

The initial stage in numerical analysis was modeling the ship and interceptor using 3D CAD design software. This research used the Aragon-2 and the dimensions of the interceptor, which were described in Table 1. Figure 1 shows the research parameters of the HUMPHREE© [15] interceptor type X350. Figure 1a presents the dimensions of the ship and the interceptor. The primary measure of the interceptor comprised the length of the span and the height of the interceptor (hi). Figure 1b describes the variation in the height of the interceptor to the stern of the ship, which comprises 100% (50 mm), 70% (35 mm), and 40% (20 mm). Figure 1c represents the position of the interceptor, which comprises close to chine, close to the keel, and at mid position. After modeling the research object, the next step was model analysis using the FVM.

### 2.2 Research method

The accuracy of the analysis used a numerical simulation that was determined by three main factors, namely convergence, grid independence, and comparison of the numerical simulation against the experiment. The calculation results at the convergence stage were obtained when they reached the identified iteration of the computer. Grid independence was an analysis with variations in the number of meshes. The comparison of the numerical simulation and the experiment shows the reasonability and reliability of the numerical results. Chapter 3.1 provides an explanation of numerical accuracy analysis.

**Table 1.** Main dimensions of the ship and the interceptor [16]

| Dimension | Full-scale | Model scale 1/5.33 | Unit |
|---|---|---|---|
| Length, overall ($L_{OA}$) | 8000 | 1500 | mm |
| Length waterline ($L_{WL}$) | 7539 | 1414 | mm |
| Breadth overall | 2300 | 431 | mm |
| Draft | 445 | 83 | mm |
| Weight | 3000 | 19.77 | Kg |
| Interceptor height (hi) | 50 | 9.37 | mm |
| Interceptor span (s) | 300 | 56.25 | mm |
| Chine breadth | 2200 | 412.75 | mm |
| Center of gravity from transom ($L_{CG}$) | 2647 | 496 | mm |
| Center of gravity from baseline ($\overline{KG}$) | 761 | 14.2 | mm |
| Deadrise angle | | 16 at transom, 24 at midship | degree |

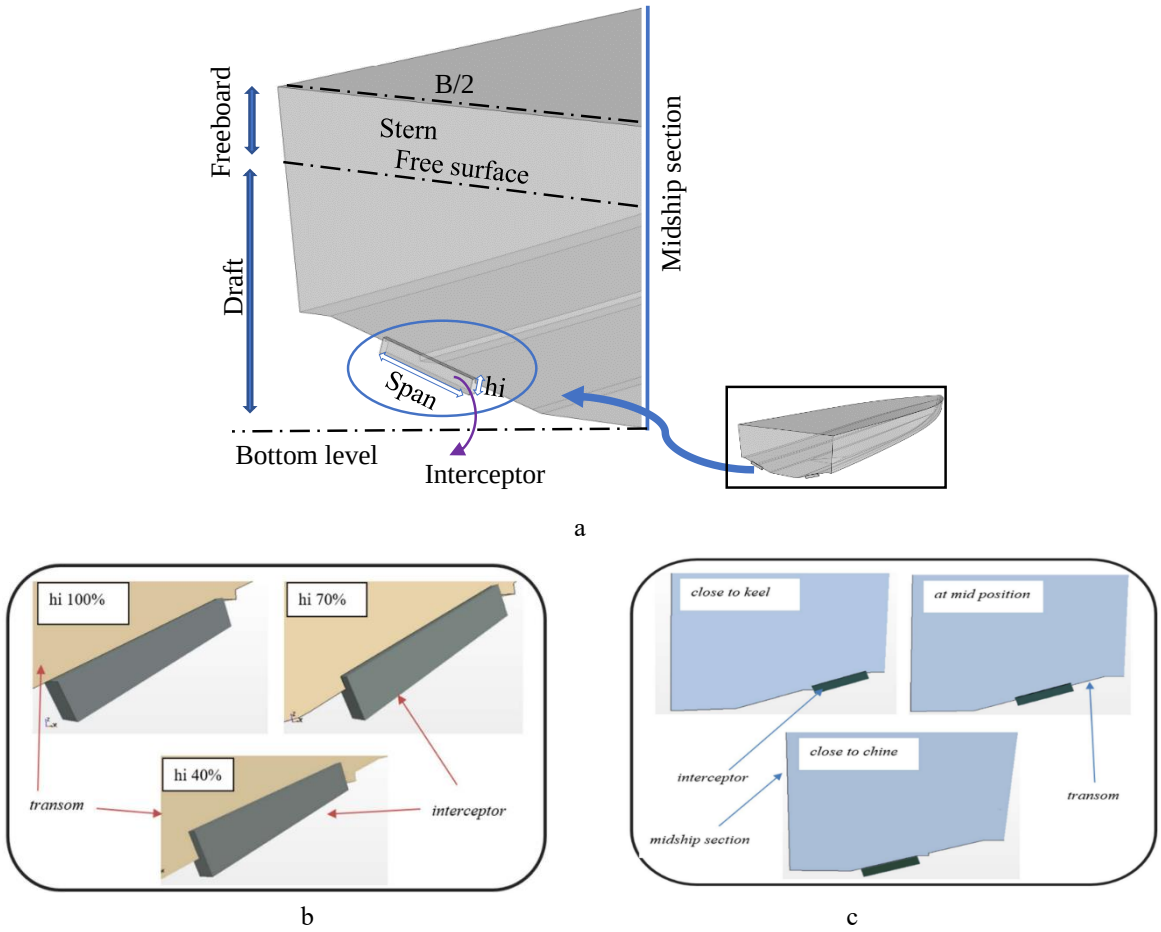


**Fig. 1** Visualization of the following: a. scheme of interceptor, b. interceptor's height, c. interceptor's positions

This research referred to the International Towing Tank Conference (ITTC), which aimed to observe the accuracy level of CFD. In this case, some of the ITTC [17] recommendations to predict high-speed craft resistance are as follows:

1. Computational domain size
2. Mesh density
3. Convergence
4. Time step
5. Grid on the ship wall ($y^+$)

Confirming the accuracy of the geometry is crucial to ensure that the surface definitions are relatively smooth and connect within a specified tolerance. Based on the length between perpendiculars ($L_{PP}$), the geometry tolerances should be set, with suitable geometric tolerance between $1 < L_{PP} < 10$. Figure 2 shows the visualization of boundary conditions and computational domains. Domain length was measured from $-2.5\ L_{PP}$ to $1\ L_{PP}$. The aforementioned visualization displayed turbulent flow behind the transom of the ship with coordinates of the zero point at the stern of the ship and the ship's draft. The water depth was 2 $L_{PP}$ ship. Furthermore, the $L_{PP}$ was the length of the ship's perpendicular. The inlet velocity condition was set in the x-negative direction, and the positive x-direction was modeled as an outlet pressure to assess the static pressure at the outlet. The upper limit was chosen as the inlet velocity to represent the unlimited air conditions. By contrast, the lower limit was chosen as the no-slip wall to explain the existence of the sea boundary. The ship was symmetrical; therefore, only half was modeled to save computational time. This approach was used by researchers to model open-sea conditions and has been shown to provide accurate results [17].

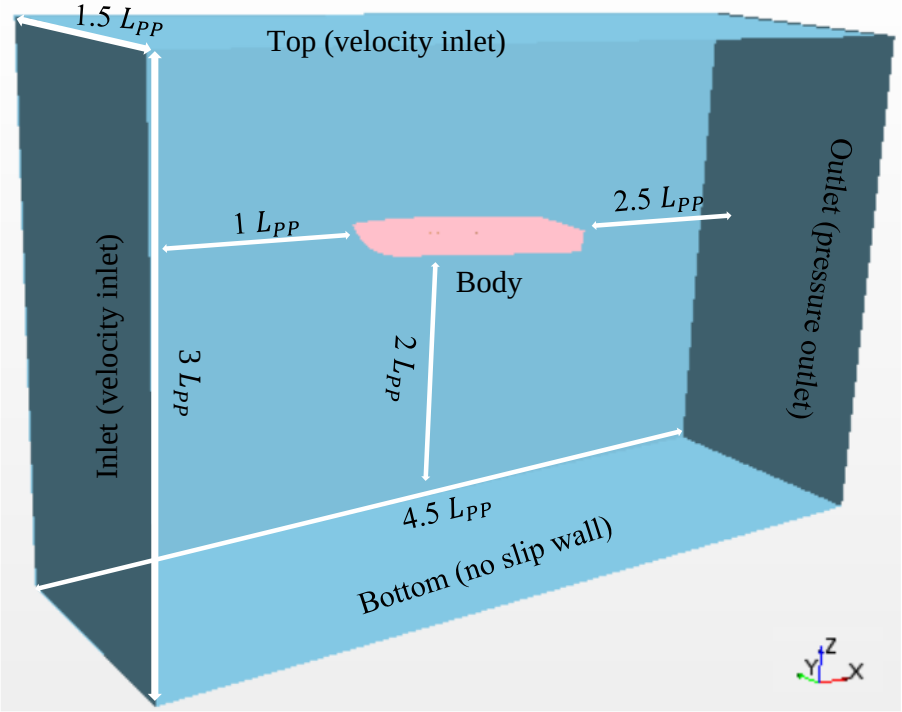


**Fig. 2** Computational domain and boundary condition

Mesh density variations were used as described in Figure 3. Variations in mesh size aimed to observe the location of concern. The density level of the mesh was focused on the free surface water and the stern of the ship due to the wash waves caused by the speed of the ship. The mesh density level could also affect the failure of the donor–acceptor mesh. Substantially high mesh density required high computational time; thus, investigating mesh density is required such that it could be used in accordance with its portion.

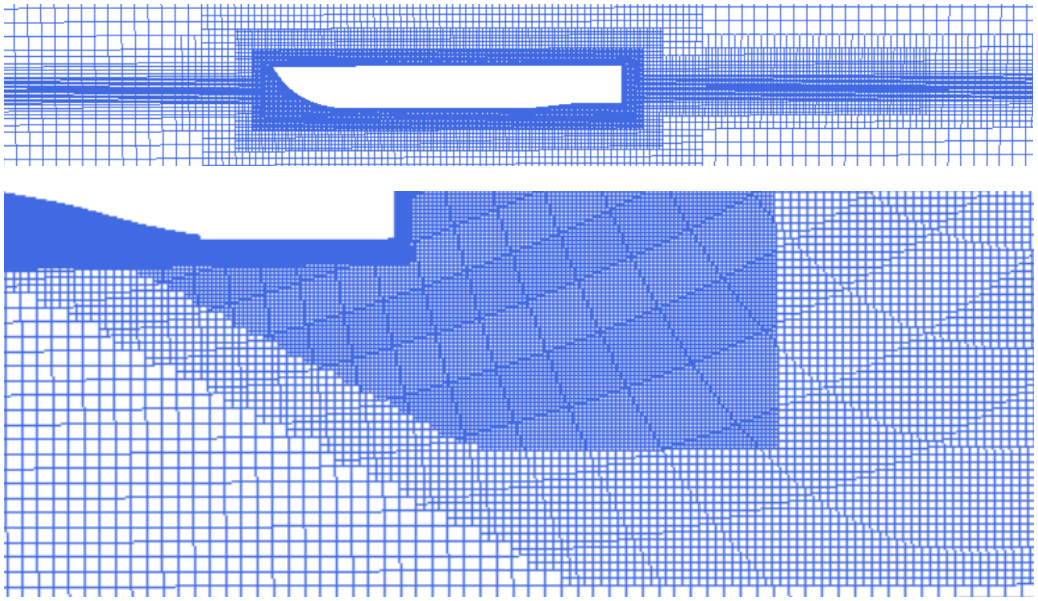

**Fig. 3** Mesh density

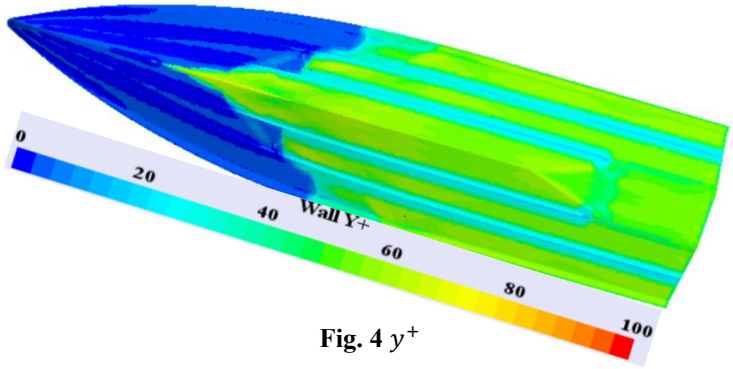


**Fig. 4** $y^+$

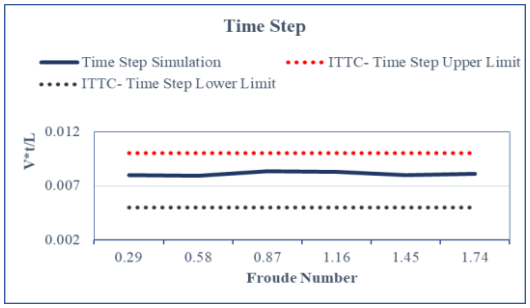


**Fig. 5** Time step selection

A variety of convergence criteria should be specified and assessed to guarantee credible solution convergence. The history of residual variations for the mass and momentum equations should be used to determine the amount of convergence. The residual shows the closeness of the existing approximate solution to the perfect mass and momentum conservation. If this requirement cannot be met due to problem complexity or oscillatory convergence, then alternative criteria, such as resistance, heave, and trim angle, can be employed.

Another parameter to validate the CFD analysis was the value of $y^+$ (wall function). The value of $y^+$ was expressed in dimensionless units to capture boundary layer phenomena. $y^+$ facilitated the easy prediction of the first layer thickness of the mesh and reduced numerical simulation inaccuracies. ITTC recommended that the value of $y^+$ was $30 < y^+ < 100$. Lotfi et al. [18] stated that the value of $y^+$ of $50 < y^+ < 150$ was still relatively good. Avci et al. [19] suggested $y^+$ to be in the 45–60 range. Figure 4 describes the value of $y^+$ between 40 and 70. The value of $y^+$, which was on the cell wall of the ship, markedly affected the friction prediction. Therefore, the thickness of the first layer must be considered to achieve the most suitable wall spacing.

The time step was the interval period for each iteration. The time step determination used the Courant–Friedrichs–Lewy number, which showed the number of points traversed by the fluid particles in the time interval. This research used a time step with a range of 0.008 in 10 s physical times, as described in Figure 5.

## 2.3 Governing equation

This research defined ship movement with dynamic fluid–body interaction (DFBI) using two degrees of freedom, free heave, and trim. Ship motions in the fluid domain were represented using rigid body motion and overset grid systems.

$$M \frac{d}{dt} \omega = n \tag{1}$$

and

$$m \frac{dv}{dt} = f \tag{2}$$

The translational and rotational motions at the center of mass of the ship model were used to trim and heave as described in Equations 1 and 2, respectively. n is the resultant moment of the ship model acting on the x-axis rotation, M is the moment of inertia of the x-axis rotation, $\omega$ is the angular velocity of the ship around the y-axis, and m is the mass of the ship, $f$ is the resultant force acting on the ship surface, and v is the ship's speed. The resultant forces and moments acting on the ship were respectively obtained from the fluid pressure and shear force on the surface of each ship. Panahi et al. [20] conducted in-depth research on this topic.

CFD was developed to predict the shape of the flow without compromising the accuracy of the calculation. Every CFD program used mathematical equations to solve fluid flows. The RANS defined mass and momentum conservation laws. The first discretization step was to divide the computational domain into a finite number of volumes via mesh formation. Next, the partial differential equations were integrated with each volume using the divergence theorem, producing an algebraic equation for each cell. This research used numerical simulations based on RANS equations to understand the performance of fast boats with and without interceptors. Equation 3 is related to the law of conservation of mass and momentum with Newtonian incompressible [21]:

$$\frac{\partial(\rho u_i)}{\partial t} + \frac{\partial}{\partial x_j}\left(\rho u_i u_j\right) = -\frac{\partial p}{\partial x_j} + \frac{\partial}{\partial x_j}\mu\left(\frac{\partial u_i}{\partial u_j} - \overline{\rho u_i{}' u_j{}'}\right) + S_j \quad (3)$$

where $u_i$ and $u_j$ are time-averaged values (i,j = 1,2,3) for the speed component, p is the time-averaged values of the pressure, $\rho$ is the density, $\mu$ is the dynamic viscosity coefficient, and $\overline{\rho u_i{}' u_j{}'}$ and $S_j$ are the Reynolds stress and source terms, respectively.

This research used the volume of fluid (VOF) method to capture changes in the water-free surface. The VOF model was well suited for simulating multiple immiscible flow phases. The fluid function of water and air depended on the volume fraction property in Equation 4, where V is the designed calculation area, V1 is the volume of fluid 1, and V2 is the volume of fluid 2. Each grid was assumed to be a volume fraction having values 1 and 0 to distinguish between air and water fluids [22].

$$\alpha(\vec{x}, t) = \begin{cases} \Delta 1, \ \vec{x}, \in V_1 \\ \Delta 0, \ \vec{x}, \in V_2 \end{cases} \quad (4)$$

For a stream comprising two different streams, $\alpha(\vec{x}, t)$ can be observed in Equation 5:

$$\frac{\partial \alpha}{\partial t} + \vec{U} . \nabla \alpha = 0 \quad (5)$$

where $\vec{U} = (u, v, w)$ is the fluid velocity. Additionally, the VOF $C_{ijk}$ function is an integral of $\alpha(\vec{x}, t)$ on each grid cell in each volume cell as described in Equation 6 below:

$$C_{ijk} = \frac{1}{\Delta v_{ijk}} \int \alpha(\vec{x}, t) \, dV \quad (6)$$

Therefore, Equation 7 was obtained as follows:

$$\frac{\partial C}{\partial t} + \vec{U} . \nabla C = 0 \quad (7)$$

where $C = 1$ for the grid that defined the fluid; $C = 0$, indicating that the grid comprised a mixture of water and air phases under the air phase and when $0 < C < 1$.

In fluid flow modeling, RANS used a predictor–corrector approach to relate the continuity and turbulence equations to the standard k-epsilon model according to the ITTC [17] recommendation. K $\varepsilon$ had two equation models comprising k and epsilon as described in Equation 8. K and $\varepsilon$ were used to define the velocity scale and turbulence scale length, respectively [21].

$$\theta = k^{1/2}, \quad l = \frac{k^{3/2}}{\varepsilon} \tag{8}$$

By using the same approach, the length of the ship model could be utilized to obtain the eddy velocity equation in Equation 9 as follows:

$$\mu_t = C\rho\theta l = \rho C_\mu \frac{k^2}{\varepsilon} \tag{9}$$

where $C_\mu$ is a dimensionless constant.

### 2.4 Overset mesh technique

The overset mesh technique is a mesh using donor–acceptor cells. This technique required more than one geometry comprising a background as a donor and an overset as a donor–recipient. Research comparing the overset and moving mesh methods was conducted in 2016. The research reported that overset mesh had better results than moving mesh [23]. Another research revealed a comparison between moving and morphing meshes and proved that the overset mesh accuracy was better than the morphing mesh. However, the overset mesh technique needs a long simulation time due to the interaction between the mesh geometries [24]. Thus, the current research used an overset mesh technique, as illustrated in Figure 6. The equations were solved separately in the two regions, and the solution was interpolated in the overlapping area comprising cells called donors and acceptors and where information was exchanged. A linear interpolation scheme was used despite its higher computational effort requirement than other available methods. This scheme minimized interpolation errors and ensured improved convergence and an accurate solution. Donor and acceptor meshes must be on the exact dimensions with insignificant differences. A significant difference caused data transfer errors; therefore, the simulation could not be completed [25].

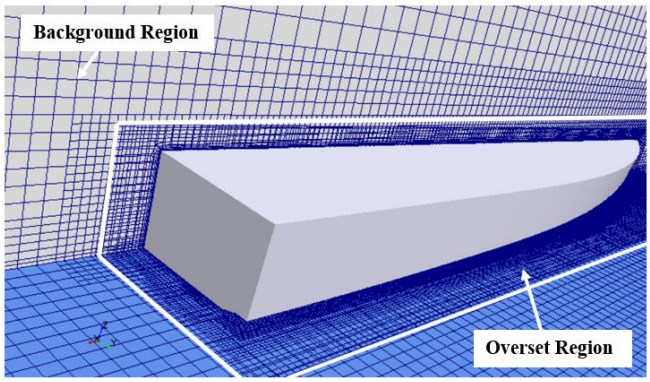


**Fig. 6** Overset technique

## 3. Result

### 3.1 Grid independence study

A grid independence study was conducted to select the most suitable mesh quantity for each simulation. The grid study reviewed the drag, trim, and heave values of the ship against five variations of mesh sizes. Analysis of the grid variation comprising 0.52, 0.66, 0.87, 1.24, and 1.47 M was performed on Froude number 1.072. M denotes million to represent the number of mesh used. The analysis was performed using a time step based on ITTC [17]. The analysis obtained a moderately convergent value on each grid but produced the most convergent value in grids 4 and 5. However, the completion of one simulation calculation was time consuming on grid 5; therefore, grid number 4 was used for all simulations. The simulation results used to observe the mesh were presented in Figure 7. An example of convergence was shown in Figure

8, representing drag, trim, and heave. The results presented in this figure were calculated using Froude Number 1.072. Moreover, the time history plotted in this figure showed that all data stabilized after 2 s; after stabilization, the simulation was stopped.

### 3.2 Convergence assessment

The CFD simulation would be compared with the research of Park et al. [16] to obtain results with reasonable accuracy. The trim, heave, and drag values showed the same pattern between CFD and the experiment. Figure 9a showed the drag error values ranging from 7.5% to 9.9%. Figure 9b demonstrated the range of trim error values of 9.27% to 10.7%. Figure 9c showed the range of error heave values between 5.7% and 10%. In the current research, a maximum difference of 10.7% was obtained, as shown on the trim graph with a Froude number of 0.87. The experimental results generally indicated that CFD could be effectively simulated, as shown in Figure 9. However, a gap in the CFD calculation was different from the experimental results. This difference was due to the limitations of CFD in modeling the environment according to actual conditions. Brizzolara & Serra [26] investigated the accuracy of CFD simulation. The research comprehensively presented the setup of the CFD model, including the type of mesh, resolution, boundary conditions, and turbulent flow model. They found that CFD could reproduce the physical phenomenon of free surface flow near the hull with an error of 10%. The Root Mean Square (RMS) error in predicting the drag to lift ratio by the numerical solution is 7.17% [27]. In some cases the accuracy of numerical calculations can be increased up to 34% [28].

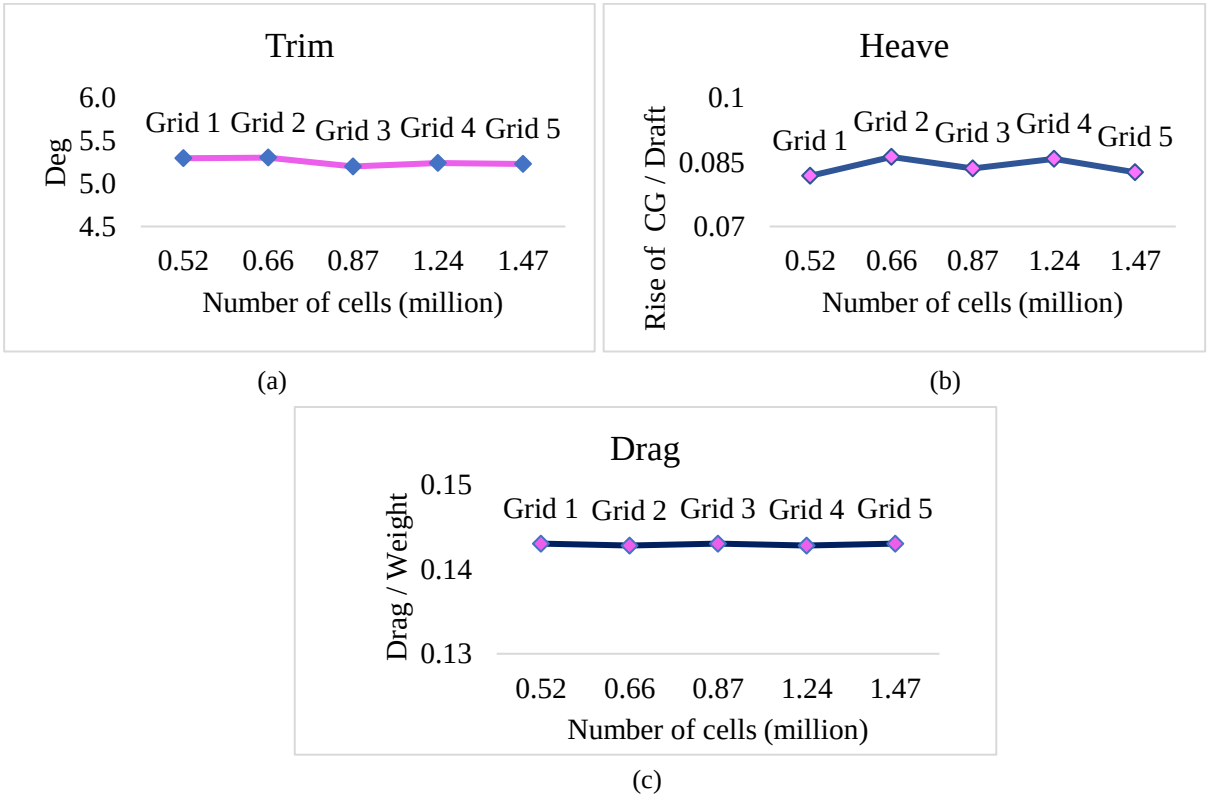


**Fig. 7** Comparison of grid convergence (a) trim, (b) heave, and (c) drag

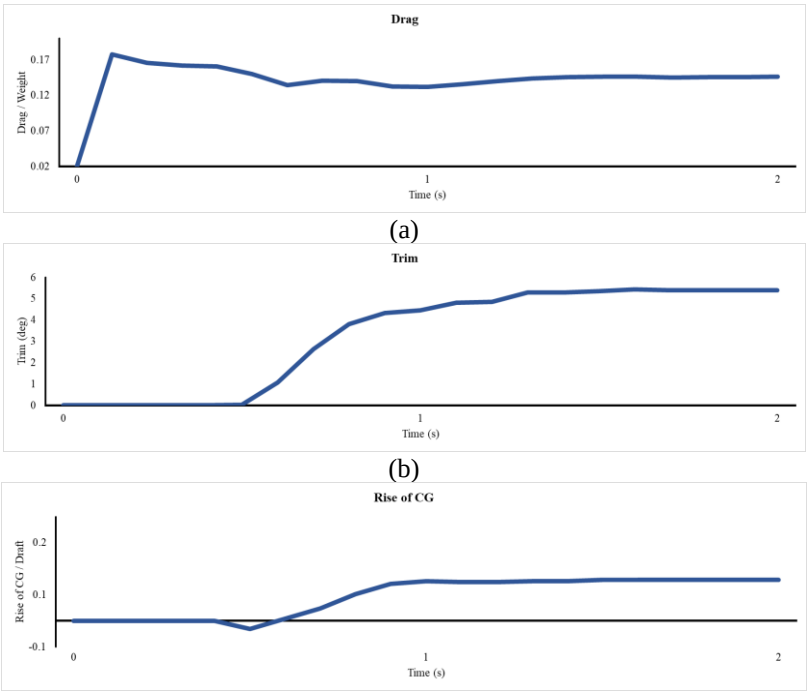


**Fig. 8** Illustration of convergence of (a) drag, (b) trim, and (c) heave parameters, demonstrating CFD model calculation of the equilibrium condition at a Froude number of 1.072.

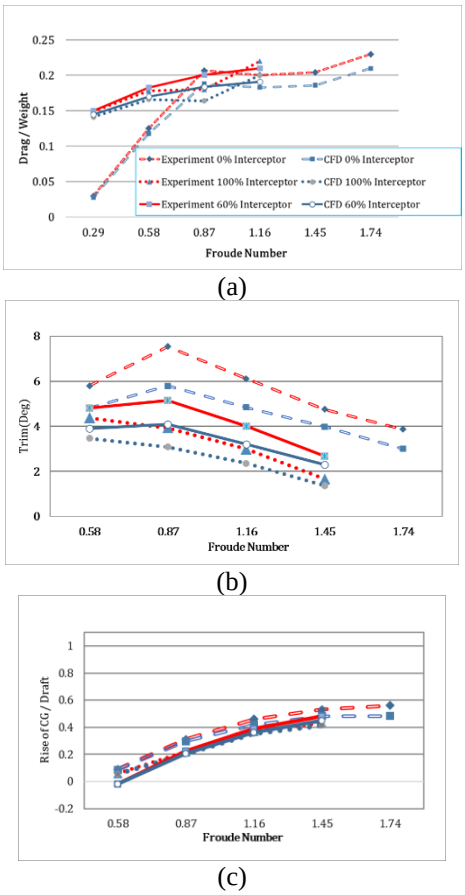


**Fig. 9** Comparison of numerical simulations of (a) drag, (b) trim, and (c) heave against the experiment measurements of Park et al. [16]

### 3.3 Simulation results

The interceptor could create flow discontinuities in the stern area of the ship. The blocked flow caused vortices and backflow effects. This phenomenon resulted in a double effect, namely an increase in lift force and the creation of a stern trim moment. Both effects reduced drag and trim of the ship. However, the speed of the ship was closely related to the pressure force generated by the interceptor. Therefore, reviewing the speed, hull shape, and appropriate interceptor height of the vessel was essential before installing this device. The controllable capability to adjust the height of the interceptor increased its effectiveness at adjusting to the desired ship speed.

Variations in the altitude and position of the interceptor caused different effects on each speed range of the ship. Close to chine, close to the keel, and at mid positions at Froude numbers 0.29 to 0.58 indicated that the interceptor was performed at an altitude of 100%, 70%, and 40%, respectively. However, in the displacement phase, the interceptor did not have a significant effect compared with the condition without an interceptor (0% interceptor). The interceptor can be used at 100%, 70%, and 40% altitudes on Froude numbers 0.87 to 1.16. This transition condition showed a drastic improvement in the trim and drag values; thus, the transition was the best condition for installing the interceptor. At Froude number 1.45, the interceptor could be used close to the keel position with a height of 100%, 70%, and 40%. The exact speed in the planing phase could be utilized close to chine and at mid positions only at an altitude of 40% of the interceptor. In Froude number 1.74, the interceptor could only be employed at an altitude of 40% for conditions close to the keel, at the mid position, and close to chine due to the dominant hydrodynamic force of the ship in the planing phase. The height of the interceptor was directly proportional to the resulting moment. Therefore, using the maximum height of the interceptor in planing conditions was not recommended because it could cause excessive moments. Reducing the interceptor height by up to 40% would produce the ideal moment to improve trim and reduce ship drag in the planing phase.

The pressure on the bottom of the ship produced by the interceptor was observed in Figure 10. This figure provided a visualization of the influence of the Froude number on the pressure generated by the interceptor. The increase in the ship's Froude number was directly proportional to the increase in pressure. The working mechanism of the interceptor can be found in Figure 11. The figure comprised the moment of the interceptor acting on the trim moment of the ship. The addition of the interceptor increased lift force, thereby reducing the trim angle.

Figure 12 describes the behavior of the planing hull ship. Displacement mode (Froude number 0.29 to 0.58) showed a hydrostatic force that caused limited extreme ship movements. The increase in the speed of the ship to the transition mode (Froude number 0.87 to 1.16) indicated the peak position of the drag and trim values. This phenomenon occurred due to the dominant hydrodynamic force acting on the ship. The trim angle increased with the speed of the ship due to the hydrodynamic forces on its bottom. The interceptor was recommended at the transition phase or the peak of the trim because the drag value in this condition is significant. Using an interceptor in the planing mode phase is not recommended because it could result in a bow-down trim due to excessive moments generated by the interceptor.

Figure 13 represents the effects of the interceptor on the ship's trim due to variations in speed. The condition of the ship without an interceptor at Froude number 1.74 showed excessive trim, causing poor ship movement. The interceptor installation at a speed of 1.74 caused the ship to experience negative trim (bow-down trim) due to excessive interceptor moments. Thus, this interceptor was declared unfit. The use of an interceptor was recommended at Froude number 0.87 to improve the most optimal trim value (fit interceptor).

The research results were shown in Figure 14 for variations of close to chine (CC), close to the keel (CK), and at mid position (MP) with 100%, 70%, and 40% conditions of interceptor height, respectively. Figure 15abc visualizes the drag results. An improvement in the drag value, namely in the Froude number 0.29 to 1.16, was observed under conditions of 100% interceptor height. However, the most effective improvement in the drag value compared to without an interceptor was found at the Froude number 0.87 with drag reduction percentages of 44%, 57%, and 52% at close to keeling, close to chine, and mid position, respectively. The drag values obtained in the 70% and 40% interceptor conditions demonstrated the same pattern as the 100% interceptor conditions, where an improvement in the drag value was found in the Froude number 0.29 to 1.16. However, the most effective improvement in the drag value was at the Froude number 0.87 with a drag reduction percentage compared to without an interceptor with a range of 43% to 51%. The best reduction in drag value was at the Froude number 0.87, close to the chine position for each interceptor height variation. The increase in total drag had no significant effect on the ship at low speeds.

The heave value can be found in Figures 14 d, e, and f. An improvement in the heave value with the same pattern for all variations was observed in the height of the interceptor. The improvement in the heave value ranged from 16% to 17%. The best heave reduction of 17% was at the Froude number 0.87, close to the chine position for each interceptor height variation.

The analysis results of the trim can be found in Figures 14 g, h, and i. The figure shows that known that the variations gave relatively the same results. The most significant change in trim value was in the close to chine position with Froude number 0.87. Compared to bare hull conditions, changes that occurred reached 8.48% whereas those at close to the keel and central position were 6.91% and 7.04%, respectively at 100%. The height of 70% and 40% demonstrated the same pattern with the most effective interceptor installation at the Froude number 0.87 and a trim value improvement from 4% to 5%. However, interceptors were not recommended at the Froude number more than 1.16 because it would cause negative trim on planing hull ships.

Figures 14 j, k, and l explained the increase in the lift force value, which was not too significant for all variations in the position and height of the interceptor. This research examined the lift force due to the hydrostatic and hydrodynamic forces of the ship. In the displacement phase, the generated lift force was due to the hydrostatic force of the ship. Meanwhile, the lift force that worked in the transition and planing phases was generated by the hydrodynamic forces of the ship. Installation of the interceptor could reduce trim and drag in the transition phase. The expected lift force value was not significantly changed due to variations in ship speed. This value was intended to represent the condition of the even keel of the ship and the improvement of the working hydrodynamic force. Thus, trim improvements would occur under the aforementioned conditions to reduce the ship's drag. The lift force value decreased without an interceptor as the Froude number increased. The most significant change in the lift force value to bare hull conditions was at Froude number 0.29 close to chine, which could change by 0.144%, and at Froude number 1.74 speed with 70% interceptor condition changes by 0.12%. Molini and Brizzolara [29] performed a flat plate simulation and applied it to the interceptor to demonstrate that the interceptor could increase the lift force. Similar studies have shown that interceptors create high lift and trim reductions by combining the position of the center of gravity with the stroke of the interceptors [3]. A lifting interceptor is the mechanism that reduces resistance for interceptors on a ship due to variations in trim and sinkage [30].

The current research revealed that the close to chine position was the most effective compared with the close to the keel and at the mid position for all variations in interceptor height at Froude number 0.87. In addition, Mansoori and Fernandes [31] indicated that if the moment produced by the interceptor was less than, greater than, or equal to the trim moment,

then the interceptor efficiency would be weak, optimal, or unfit for use, respectively. The trim of the ship was not well controlled on an interceptor with weak efficiency. Meanwhile, an unfit interceptor could result in negative trim while increasing the ship's drag.

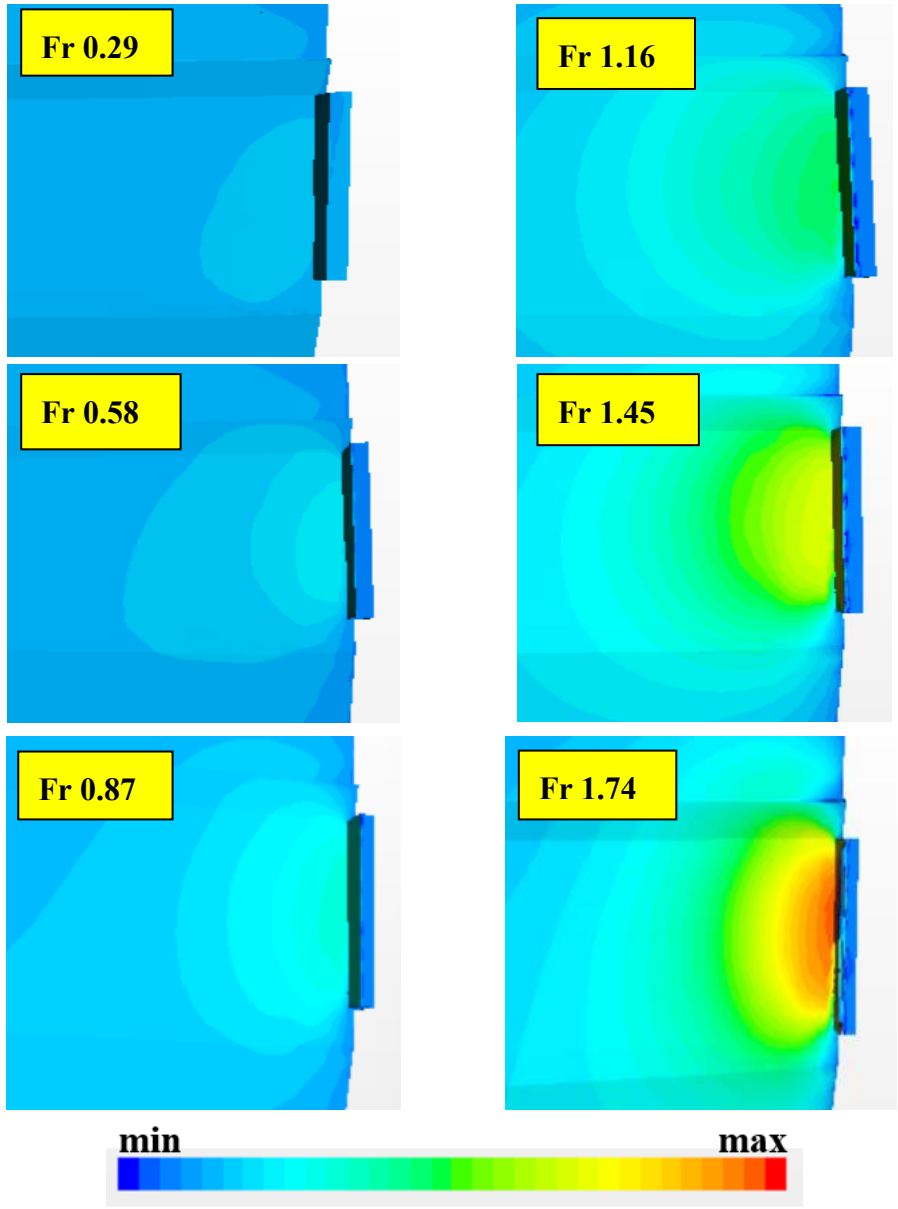


**Fig. 10** Pressure Distribution at 100% interceptor (Close to Chine)


**Fig. 11** Moments and forces generated by the interceptor

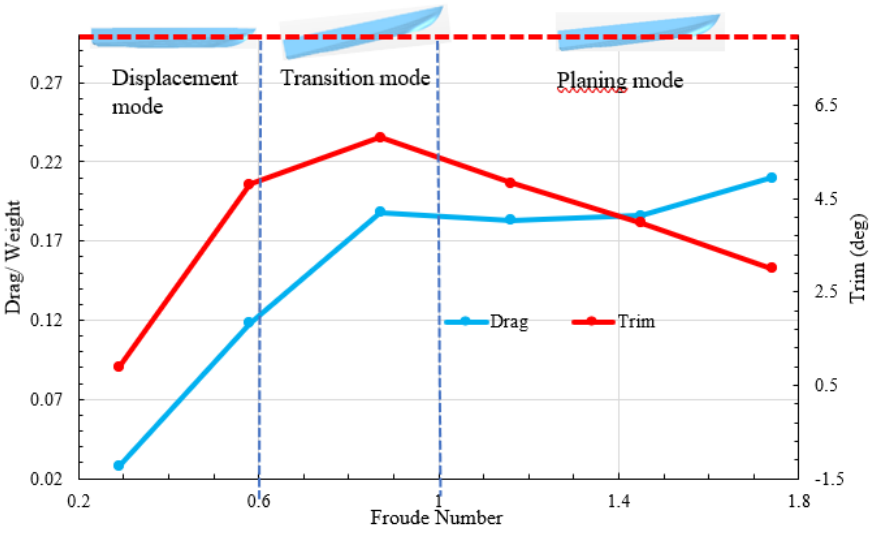


**Fig. 12** Interceptor installation region

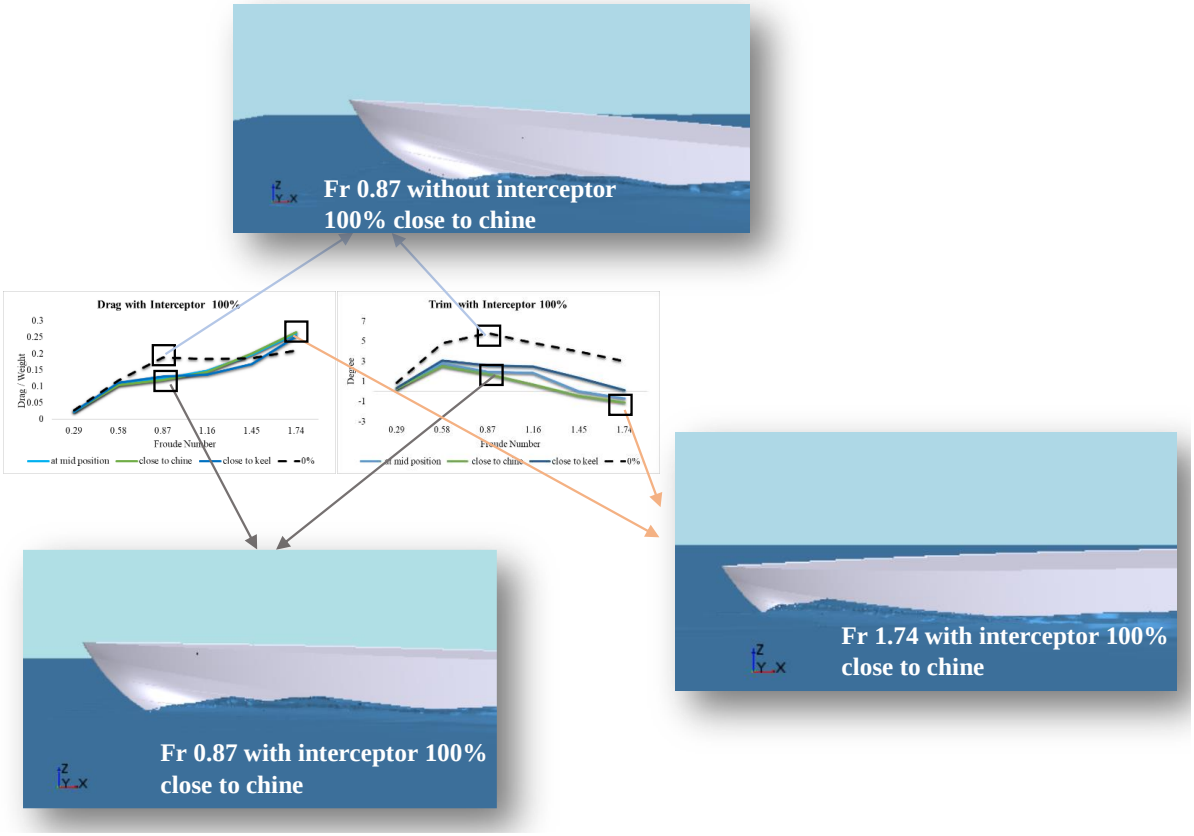


**Fig. 13** Trim control by interceptor

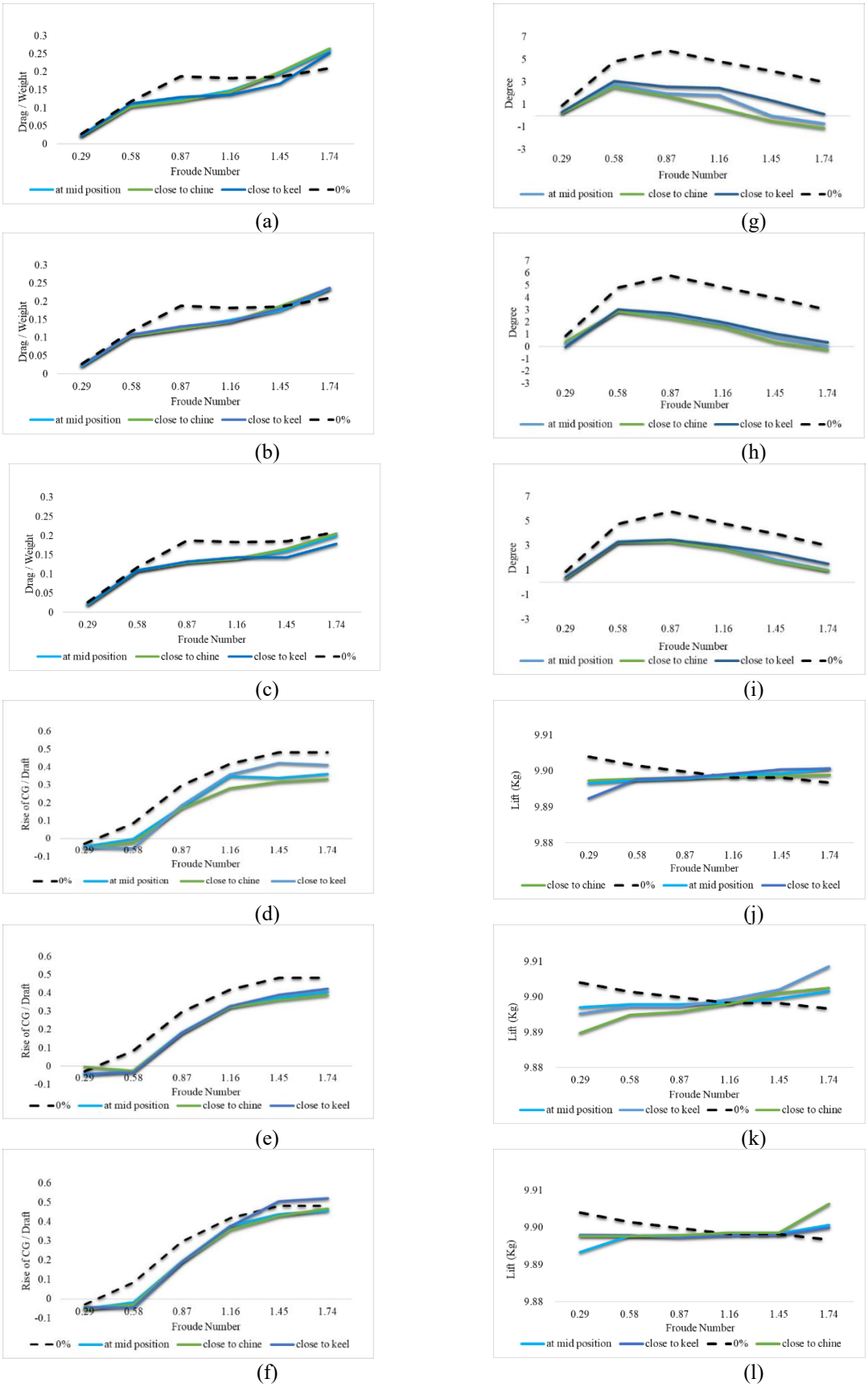


**Fig. 14** Interceptor effects: (a) drag 100% interceptor, (b) drag 70% interceptor, (c) drag 40% interceptor, (d) heave 100% interceptor, (e) heave 70% interceptor, (f) heave 40% interceptor, (g) trim 100% interceptor, (h) trim 70% interceptor, (i) trim 40% interceptor, (j) lift force 100% interceptor, (k) lift force 70% interceptor, and (l) lift force 40% interceptor

## 4. Conclusion

This research mainly aimed to provide information on the interceptor's design on the planing hull. This research studied the effects of changing interceptor position and height simultaneously, thus affecting trim, heave, drag, and lift force.

This research reported a numerical study by showing the grid independence study. The results of the numerical simulation study were compared with the experimental results conducted by Park et al. The level of accuracy of CFD provided relevant results to the experiment with a maximum difference of 10.7%.

Applying an interceptor on a planing hull vessel could generally reduce the trim angle of the vessel, resulting in a low draft height and drag force. Implementing the interceptor would directly change the pressure on the bottom of the ship and change the created moment. The pressure in the interceptor area would also increase with ship speed. The interceptor installation on fast boats was intended for transition areas due to the substantial increase in the trim angle of the ship followed by the drag. If the moment on the interceptor (Mi) was more significant than the trim moment (Mt), then the ship would experience negative trim. This condition would endanger the ship. Thus, interceptors at high speeds were not recommended for use.

This research reported that interceptors at close to chine, close to the keel, and at mid position locations positively affected the 0.29 to 1.16 Froude number. The results of this test showed that the drag value at close to chine with an interceptor height of 100% was the most effective. The best condition occurred at Froude number 0.87 with a percentage reduction of 57% drag, 17% heave, 8.48% trim, and 0.12% lift force compared to no interceptor.

The comparison of interceptor positions did not significantly change the performance of the ship. The drag value was reduced by 0.4% and 1.1%, trim by 0.06% and 0.24%, and heave by 0.1% and 0.2% at the mid position and close to the keel at Froude number 0.87.

The difficulty in determining dynamic trim is solely related to the problem in identifying pressure distribution on the hull bottom. Pressure distribution is affected by the hydrodynamic lift of the hull. These findings highlight the importance of accurate geometry and hydrostatic data when making simulation predictions.

## Acknowledgments

The authors would like to thank Prof. Dong-Joon Kim and Professor Jong-Yong Park (Pukyong National University) for providing the experimental data used in this study. We would like to express our gratitude to LPPM Universitas Diponegoro for providing professional English proofreading services.

## REFERENCES

[1] Uithof. K., Oossanen. P. Van, Moerke. N., Oossanen. P. G. Van., Zaaijer. K. S., 2002. An Update on the Development of the Hull Vane. *9th International Conference on High-Performance Marine Vehicles (HIPER).* Athens.

[2] Hou. H., Krajewski. M., Ilter. Y. K., Day. S., Atlar. M., Shi. W., 2020. An experimental investigation of the impact of retrofitting an underwater stern foil on the resistance and motion. *Ocean Engineering*, 205, 107290. https://doi.org/10.1016/j.oceaneng.2020.107290

[3] De Luca. F., Pensa. C., 2012. Experimental investigation on conventional and unconventional interceptors, *Transactions of the Royal Institution of Naval Architects Part B: International Journal of Small Craft Technology*, 154, PART B2. https://doi.org/10.3940/rina.ijsct.2012.b2.129

[4] De Luca. F., Mancini. S., Manfredini. A., Pensa. C., Scognamigli. R., 2015. Interceptor Device for a High-speed Displacing Craft (Comparison between CFD Simulation and Experimental Data), *18th International Conference on Ships and Shipping Research, NAV 2015*, pp. 906–915.

https://doi.org/10.13140/RG.2.1.3047.9842
[5] Rijkens. A., Cleijsen. H. M. A., Keuning. J. A., 2013. On the hydrodynamic performance of an Improved Motion Control Device for Fast Ships, *12th International Conference of Fast Sea Transportation*, Delft, Netherlands
[6] Mansoori M., Fernandes A. C., 2017. Interceptor and trim tab combination to prevent interceptor's unfit effects. *Ocean Engineering,* 134, 140–156. https://doi.org/10.1016/j.oceaneng.2017.02.024
[7] Mansoori. M., Fernandes A. C., 2016. The interceptor hydrodynamic analysis for controlling the porpoising instability in high speed crafts. *Applied Ocean Research*, 57, 40–51. https://doi.org/10.1016/j.apor.2016.02.006
[8] Jangam. S., Sahoo. P., 2021. Numerical investigation of interceptor effect on seakeeping behaviour of planing hull advancing in regular head waves. *Brodogradnja*, 72, 73–92. https://doi.org/10.21278/brod72205
[9] Karimi. M. H., Seif. M. S., Abbaspoor. M., 2013. An experimental study of interceptor's effectiveness on hydrodynamic performance of high-speed planing crafts. *Polish Maritime Research*, 20, 21–29. doi: 10.2478/pomr-2013-0013. https://doi.org/10.2478/pomr-2013-0013
[10] Yousefi. R., Shafaghat. R., Shakeri. M., 2013. Hydrodynamic analysis techniques for high-speed planing hulls. *Applied Ocean Research,* 42, 105–113. https://doi.org/10.1016/j.apor.2013.05.004
[11] Samuel. S., Iqbal. M., Utama. I. K. A. P., 2015. An investigation into the resistance components of converting a traditional monohull fishing vessel into catamaran form. *International Journal of Technology,* 6, 432–441. https://doi.org/10.14716/ijtech.v6i3.940
[12] Samuel. S., Kim. D. J., Iqbal. M., Bahatmaka. A., Prabowo. A. Rio. Bulbous Bow Applications on a Catamaran Fishing Vessel for Improving Performance, *MATEC Conference.* Bali, Indonesia. https://doi.org/10.1051/matecconf/201815902057
[13] Firdhaus. A., Suastika. I. K., Kiryanto. K., Samuel. S., 2021. Benchmark study of FINETM/marine CFD code for the calculation of ship resistance. *Kapal Jurnal Ilmu Pengetahuan dan Teknologi Kelautan.* 18, 111–118. https://doi.org/10.14710/kapal.v18i2.39727
[14] Sukas. O., Kinaci. O. K., Cakici. F., Gokce. M. K., 2017. Hydrodynamic assessment of planing hulls using overset grids. *Applied Ocean Research*, 65, 35–46. https://doi.org/10.1016/j.apor.2017.03.015
[15] Humphree, 2022. Interceptor Series. https://humphree.com/. accessed 8th August 2021.
[16] Park. J. Y., Choib. Hujae., Leec. Jooho., Choid. Hwiyong., Wooe. Joohyun., Kimc. Seonhong., Kimb. Dong Jin., Kimb. Sun Young., Kim. Nakwan., 2019. An experimental study on vertical motion control of a high-speed planing vessel using a controllable interceptor in waves, *Ocean Engineering.* 173, 841–850. https://doi.org/10.1016/j.oceaneng.2019.01.019
[17] ITTC., 2011. Practical guidelines for ship CFD applications. *ITTC – Recommendation Procedure Guideline* 1–8.
[18] Lotfi. P., Ashrafizaadeh. M., Esfahan.R. K,. 2015. Numerical investigation of a stepped planing hull in calm water. *Ocean Engineering.* 94, 103–110. https://doi.org/10.1016/j.oceaneng.2014.11.022
[19] Avci. A., Barlas. B., 2019. An experimental investigation of interceptors for a high speed hull. *International Journal Naval Architecture and Ocean Engineering.* 11, 256–273. https://doi.org/10.1016/j.ijnaoe.2018.05.001
[20] Panahi. R., Jahanbakhsh. E., Seif. M. S., 2009. Towards simulation of 3D nonlinear high-speed vessels motion. *Ocean Engineering.* 36, 256–265. https://doi.org/10.1016/j.oceaneng.2008.11.005
[21] Wilcox. D. C., 1994. Simulation of transition with a two-equation turbulence model, *AIAA Journal*, 32, 247–255. https://doi.org/10.1016/j.oceaneng.2008.11.005
[22] Hirt. C.W., Nichols. B. D.,1979. Volume of fluid (vof) method for the dynamics of free boundaries. *Journal of Computational Physics*. 39,201-225. https://doi.org/10.1016/0021-9991(81)90145-5
[23] De Luca. F., Mancini, S., Miranda, S., Pensa. C., 2016. An extended verification and validation study of CFD simulations for planing hulls. *Journal Science Research,* 60, 101–118. https://doi.org/10.5957/jsr.2016.60.2.101
[24] De Marco. A., Mancini. S., Miranda. S., Scognamiglio. R., Vitiello. L., 2017. Experimental and numerical hydrodynamic analysis of a stepped planing hull. *Applied Ocean Research.* 64, 135–154. https://doi.org/10.1016/j.apor.2017.02.004
[25] Samuel. S., Trimulyono. A., Manik. P., Chrismianto. D., 2021. A numerical study of spray strips analysis on fridsma hull form. *Fluids*. 6. https://doi.org/10.3390/fluids6110420
[26] Brizzolara. S., Serra. F., Accuracy of CFD Codes in the Prediction of Planing Surfaces Hydrodyamic Characteristics. *2nd International Conference Maritime Research Transportation.* Italy
[27] Roshan.F., Dashtimanesh. A., Bilandi. R. N. 2020. Hydrodynamic characteristics of tunneled planing hulls in calm water. *Brodogradnja*, 71, 19–38. http://dx.doi.org/10.21278/brod71102
[28] Ahmed. T. M.., Elaghbash. A. O., Banawan.A. A., Ahmed.Y. M., Hassan. A. M. 2020. Numerical prediction of solitary wave formation of a planing hull in shallow water channels. *Brodogradnja*, 71, 135–

148. http://dx.doi.org/10.21278/brod71308
[29] Molini. A., Brizzolara. S., 2005. Hydrodynamics of interceptors: a fundamental study. *International Conference on Maritime Research and Transportation*. Italy.
[30] Day. A. H., Cooper. C., 2011. An experimental study of interceptors for drag reduction on high-performance sailing yachts, *Ocean Engineering*. 38, 983–994, https://doi.org/10.1016/j.oceaneng.2011.03.006
[31] Mansoori. M., Fernandes. A., Ghassemi. H., 2017. Interceptor design for optimum trim control and minimum resistance of planing boats. *Applied Ocean Research.* 69, 100–115. https://doi.org/10.1016/j.apor.2017.10.006

Submitted: 20.06.2022.
Accepted: 03.09.2022.

S Samuel, Assistant Professor, Department of Naval Architecture, Universitas Diponegoro, Semarang, Indonesia
Ocid Mursid* (ocidmursid@lecturer.undip.ac.id), Assistant Professor, Department of Naval Architecture, Universitas Diponegoro, Semarang, Indonesia
Serliana Yulianti, Research Scholar, Department of Naval Architecture, Universitas Diponegoro, Semarang, Indonesia
Kiryanto, Associate Professor, Department of Naval Architecture, Universitas Diponegoro, Semarang, Indonesia
Muhammad Iqbal, PhD candidate, Department of Naval Architecture, Ocean, and Marine Engineering, University of Strathclyde, Glasgow, UK, United Kingdom